An Appalachian automated dual axis solar tracker and analysis

Brian W Myer
Appalachian State University
525 Rivers St
Boone, NC 28608
E-mail: myerbw@appstate.edu

Nathan Kelischek
James Phillips
Sterling Herron
Daniel Richard
John Markham
James P Sherman
Department of Physics & Astronomy
Appalachian State University
525 Rivers St
Boone, NC 28608

Algarve Energy Park
Vale da Rainha, Estrada de Monchique
Rasmalho CCI no 20, 8500-827 Portimão
Portugal

ABSTRACT

Today's young scientists and engineers need practical experience with tracking techniques appropriate for solar. Tracking systems are not fully developed right now, although many trackers are in development and on the market. With a minimal budget, a system was designed and built from scratch, integrating control, tracking and performance monitoring.

Broadband direct and diffuse irradiances were also modeled in REST2 to compare with measured output performance, using as inputs atmospheric parameters acquired at Appalachian State University's AERONET site (APPALACHIAN_STATE). A simple non-linear model for photovoltaic panel operation was implemented using the IVFIT and IVGEN routines.

The promising preliminary results of this student project are presented, as well as lessons learned on and off sun at Appalachian State University in the mountains of Boone, NC.

1. INTRODUCTION

According to the National Academy of Engineering, harnessing fusion, carbon sequestration, and even providing clean water to the billions without access all rely on making solar energy affordable [1]. In 2009, the United States domestic solar market grew to be third largest in the world, with over 1250 Megawatts Photovoltaic (PV) and 431 Megawatts Concentrating Solar Power. However, solar was still lost in 'other renewables' at a fractional percent of total US energy production [2]. Trimming down the peak load on the existing grid will decrease overall consumption. Two major challenges for the significant advancement of solar technology's use: payback period is too long, and capital expenses are too high. Double-digit efficiency, 180 Watt, PV panels can cost up $800 each. Alone, novel, 30%+ efficiency PV cells cost too much to manufacture for terrestrial use due to the materials. Tracking can improve the returns for efficient panels and also enables concentrators.

To maximize effectiveness, PV panels are often directed due South at a tilt angle that corresponds to latitude. In this orientation, panels might typically produce at maximum output for 3 hours on a clear day in summer. To build significantly large systems, PV panels are being integrated into buildings horizontally, to avoid shading and spacing. On such days, a PV panel placed on the dual-axis tracking system reported here generated 79% more Wh of energy than an identical fixed panel tilted at latitude.

This report describes the construction of the tracking and monitoring system, development of the tracking algorithm, and examination of power performance data beside atmospheric measurements. This is presented in the context of a collaborative research project including high school and college students engaged in the NSF supported Academy of Sciences Applied Solar Energy Research Cluster at Appalachian State University (AppState).

2. BUILDING THE TRACKER SYSTEM

During fall 2009, development began on a solar tracking system with a team at AppState. The system was installed and tested autonomously on a campus rooftop during summer 2010.

A dual axis tracking system typically consists of two orthogonal drives, one each for azimuth and elevation angles. In this case azimuth was the primary axis, supporting the elevation drive, which in turn supported the panel. Each drive requires a motor and encoder on an axle. Cabling connected the tracker and controller, harnessed to the elevation plate to allow freedom of movement. The support post allowed for field leveling adjustment.

2.1 Mechanical System

The tracker system implemented consisted of automotive flywheel gears with bearings welded to a post, and a fork. The post was tapped with screws to allow for leveling and orientation when slipped over a slightly smaller diameter base (Fig. 1).

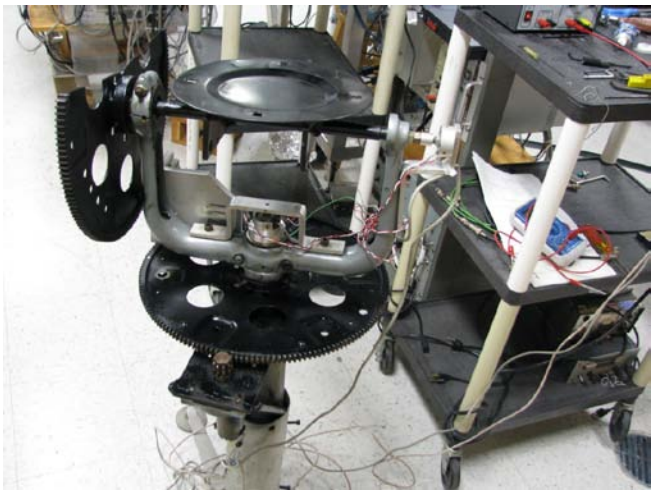

Fig. 1: Mechanical tracking system, showing automotive gears, pots, mount, and wiring for reading pot voltages.

Before motors were installed the assembly would swing and rotate freely. Mechanical resistance of the un-energized motors was the only braking force. This is a reliability issue in terms of surviving wind gusts, especially for large trackers with areas of tens of square meters, and must be treated in detail in those cases.

2.2 Motors

Nominal 32 VDC gear motors, from a satellite dish tracker were used. This kind of motor can be driven in either direction based on applied voltage polarity.

To familiarize students with motor function, a safe laser pointer was mounted to the elevation plate; then, DC power supplies were connected to each motor with switches, so that a pair could manually drive the light spot along a target curve drawn on the board. Following the light with chalk made a nice illustration of tracking accuracy and corrections.

2.3 Angle Encoding

Encoding of angular position used 100Ω potentiometers located axially to azimuth and elevation. These three-legged pots were used as voltage dividers, with an input nominal 5V applied across the outer legs, while output voltage between the middle and an outer leg varied with drive position. After testing, voltage variation with angular position was found to be adequately repeatable and linear to allow relation using one linear equation for each axis. To obtain best accuracy, it is necessary to monitor both the input and output voltages. Usually, a rotary encoder is a better option.

Tracking systems for concentrators have different requirements for accuracy, and siting may require characterization of the encoder at every position and employment of lookup tables. Concentrated solar energy trackers fill a middle ground between research telescope trackers with precise optically read bar encoding and the basic pot method used here.

Correction of tracking using a light sensor was not implemented in this open-loop control algorithm. Several solar energy tracking projects have been developed in the department of Physics & Astronomy at AppState in recent years [3,4,5], one of which used a webcam and image processing as the closed-loop part of a hybrid routine.

2.4 Controller

The Arduino Duemilanove microcontroller was used with the Ardumoto shield (Fig. 2). Some experimentation was performed with a homemade MOSFET motor driver circuit, but it was unreliable. The Ardumoto shield provided a convenient digital to analog interface suitable for operation with a 12V battery and the nominal 32VDC motors.

As the project was not focused on computer programming, the high level C programming used with this controller significantly facilitated progress with controls for students with no prior coding experience.

The control code and associated ideas will be posted on the appropriate Arduino forum, whose assistance this project benefitted greatly from [6].

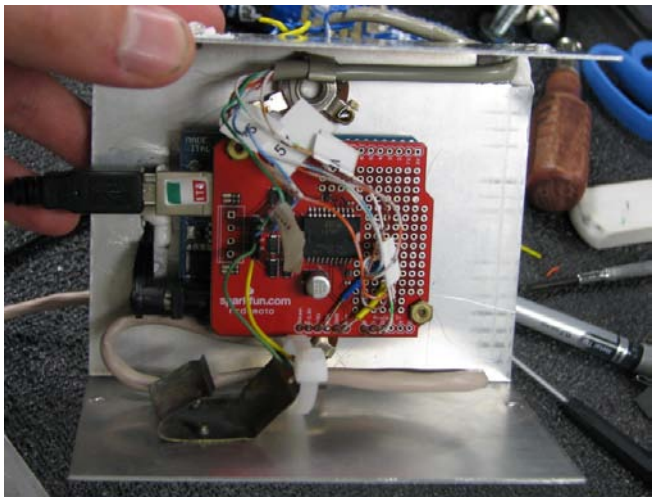

Fig. 2: Microcontroller interfaced with motor driver shield, motors, encoding pots and USB for program upload.

Student control development began with testing existing code for timing and motor control, then combining functions to realize more complex algorithms. Four defined analog output pins drove two motors used. The motors independently and in turn directed the panel to target pot voltages representing sun azimuth and elevation angles.

2.5 Sun Position

Defining time and solar position for a tracking system requires a time reference. Initially, a table defined a 'day' of times and target azimuth/elevation pairs 10-15 minutes long.

A 'lab calibration' was performed by reading the pot voltages while varying the angular position of the mount, checked with a spirit level. For example, 3.98V and 1.14V corresponded to azimuthal West and East, respectively. Defined angles and measured voltages were plotted by hand on a large piece of graph paper where the linear relationship was clear, and the slope and intercept obtained agreed to two decimal places with a computerized linear regression. These parameters were used to convert calculated sun positions to target tracker voltages.

The sun position calculations employed the equations from the NOAA Solar Position Calculator spreadsheet, and the APPALACHIAN_STATE site latitude (36.2N), longitude (81.7W) and time zone (UTC -4 during Summer 2010) [7].

In order to move the system to the field site, it was necessary to orient and calibrate the angular positions and work in a consistent time system.

For daily functionality without constant oversight, time must be defined, in this case UNIX time, expressed as the number of seconds since Jan 1, 1970 at 12:00 hours. Once synchronized to a local or UTC time, the Arduino clock kept adequate time with the function now() accessing controller time.

3. PHOTOVOLTAIC PANELS

Two monocrystalline silicon 50W panels were purchased for testing. The STC characteristics of the panels are listed in Table 1.

Table 1 STC Panel Characteristics

Nominal Power (W)	50.0
Voc (V)	21.6
Isc (A)	3.23
Vmpp (V)	17.2
Impp (A)	2.91

Using approx. 100W wire wound resistors, current-voltage (i-v) characterization was performed outdoors.

This confirmed their identical performance and determined 5.7Ω as the maximum power point (MPP) load.

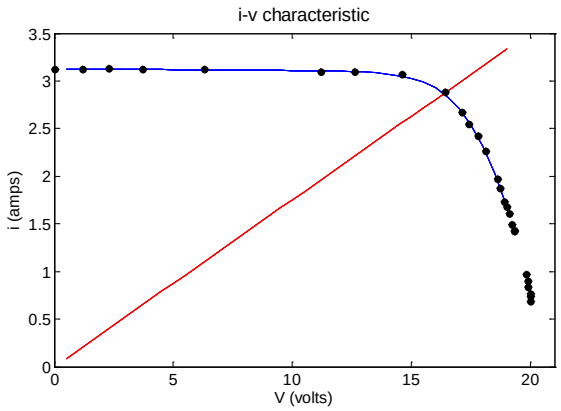

Fig. 3: Current-voltage characteristic of PV panels used, for global irradiance 944W/m^2, temperature 30°C.

One PV panel was then mounted to the tracking system and both panels connected across 5.7Ω resistors, intended to obtain optimal power for the tracker.

One common pitfall in PV testing is to measure only Voc and Isc taking the product as power out. As the panel outputs were not 'inverted', fixed resistive loads were used to allow measurement of power actually delivered. Discussion in this context helps show students why short circuit and open circuit conditions deliver ideally no power and can not exist at the same time, for either electrical or mechanical loads. Furthermore, panels delivering power to the optimal load suffer minimal internal heating, improving validity of the performance test [8]. Another benefit from a monitoring perspective is that, given the resistance, a single voltage measurement determines voltage and current. Wirewound resistivity temperature coefficients are on the order of one part per thousand per degree temperature change, so variation of resistance value was neglected.

3.1 Field Calibration

On several clear days, a current meter was connected across the panel leads to measure short circuit current (Isc), and position calibrated by driving the tracker to maximize Isc. By recording encoder voltages and the controller time, the relationship between voltages and sun position was determined. For angular position, the slope relationships, or mV/deg do not vary, and only the intercepts or offsets reflect the new tracker orientation.

This alignment procedure needs to be repeated periodically or when there is a mechanical change in the system [9].

The algorithm was written to track every 10 minutes, and record and log voltages every two minutes.

In order to read the loaded panel voltages at the controller 5V analog inputs voltage dividers 1 : 4.6 were used. The calibration of the voltage dividers was tested by measuring directly across the panels with a meter and comparing with simultaneous logged values.

4. PERFORMANCE

The fixed PV panel, identical to that on the tracker, was tilted at latitude and due South, and collocated (Fig. 4). Data for each of the panels were saved from the serial HyperTerminal via USB on a laptop located in a container below the panels, on the Broyhill Center roof at AppState.

Fig. 4: Test site: fixed panel in foreground, tracker in background beside AppalAir atmospheric instruments [10].

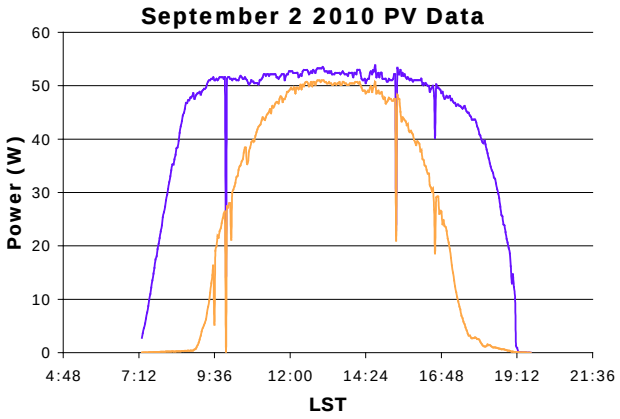

Fig. 5: Panel output power comparison for a relatively clear day. Tracking panel daily energy production was 64% higher than fixed panel. Sharp dips indicate quickly passing clouds.

Load voltages were calculated from monitored voltages using the divider calibration. Panel output powers were then calculated from the 2-minute load voltage values and measured resistor values (Figs. 5 and 6).

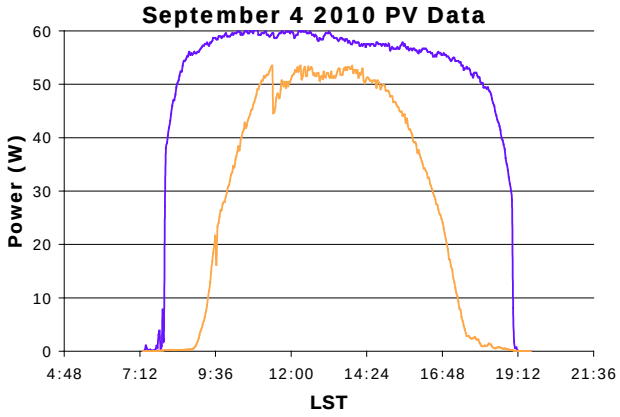

Fig. 6: Power produced by the tracking panel vs. the fixed panel. Integration reveals that tracking led to 79% more energy production over the day.

Notable in both Figs. 5 and 6 above, are large slopes in output power curves at low sun elevations. These are explained by the combination of changing irradiance and fixed load resistances.

5. MODELING

During the experiments described above, no irradiance monitoring was conducted. Fortunately, the tracker was installed beside an operational CIMEL Sunphotometer linked to AERONET (APPALACHIAN_STATE site) and thus the REST2 model was used to simulate the irradiance conditions at our PV test site during operation [11,12,13].

Irradiance estimates and i-v data were then input to IVFIT and IVGEN routines to obtain estimated i-v curves for each time step. Panel output power was obtained as intercepts of i-v curves with load curves [14,15].

5.1 Irradiance Modeling

This CIMEL measures sun and sky radiance in seven bands between 340nm and 1020nm, from which aerosol spectral optical depth (AOD) is directly determined. Measurements are made at regular relative air mass intervals along cloudless lines-of-sight. Solar radiance measurements in the 870nm and 936nm bands are used to derive precipitable water vapor (units:cm) and NO2 and O3 columns in Dobson units (DU), with 1 DU = 0.001 atm-cm [16].

In Fig. 7 below, AOD time series are plotted in the 7 bands.

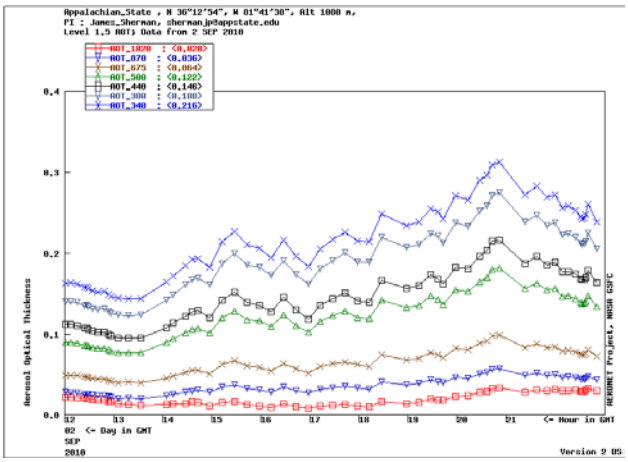

Fig. 7: Spectral AOD data, APPALACHIAN_STATE AERONET measurement site, on 2 Sept. 2010.

The correlated, nearly parallel nature of the curves in Fig. 7 suggests a parameterization as a function of wavelength and a spectrally dependent aerosol Bougher-Beer-Lambert law model is implemented in REST2 as:

(1) $$T_{a\lambda} = \exp(-m\,\tau_{a\lambda})$$

where $T_{a\lambda}$ is spectral aerosol transmission, m is the air mass, and $\tau_{a\lambda}$ is spectral optical depth. A double logarithmic plot of wavelength and AOD shows a linear relationship, which is parameterized by Gueymard as:

(2) $$\ln(\tau_{a\lambda}) = -\alpha_i \ln(\lambda) + \ln(\beta_i)$$

where α is the angstrom wavelength exponent, β is AOD at 1um, and subscripts indicate fits to two bands: band 1 includes wavelengths shorter than 0.7um and band 2 wavelengths longer than 0.7um (Fig. 8).

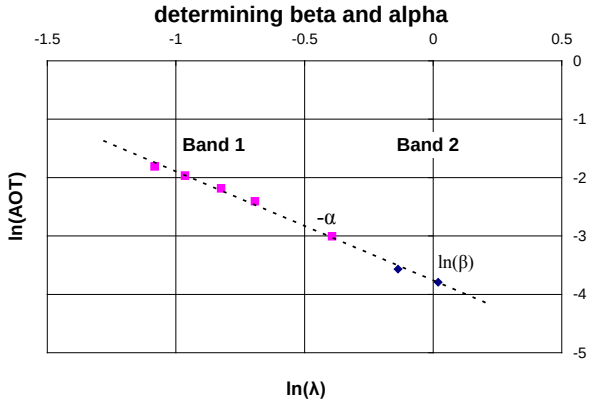

Fig. 8: Determination of broadband (α, β) with (α = 1.94, β = 0.02) from slope and intercept (-1.94, -3.91) for a single time step.

As the site AOD data only offer two points in band 2, a linear fit for band 2 is not appropriate. The physical constraint that both curves have the same value at 0.7um in principle facilitates evaluation of the segmented linear regression but instead here the parameters were extracted as one broadband (α, β) pair at each measurement time step.

Although a broadband fit was analyzed, the REST2 model was used in particular because it allows alpha to deviate from 1.3 and models diffuse as well as direct radiation as in Figs. 8 and 9.

A summary of parameters estimated for one day is presented in Table 2, compared with REST2 default values. Atmospheric pressure, p, shown is not a global default, but based on site altitude and latitude inputs.

Table 2 Model Parameters for REST2, 2 Sept. 2010

Parameter	REST2 Defaults	Experimental
p (pressure, hPa)*	891.8	897.5 ± 0.7
w (water, cm)	1.5	1.38 ± 0.21
uo (O3, atm-cm)	0.3	0.298 ± 8 E-5
un (NO2, atm-cm)	0.0002	0.000175 ± 6 E-8
α	1.3	2.13 ± 0.20
β	n/a	0.025 ± 0.008
pi1 (scatter albedo 1)	0.95	n/a
pi2 (scatter albedo 2)	0.90	n/a
rog (regional albedo)	0.2	n/a

One day's modeled irradiances are shown in Fig. 9. As noted below in section 5.2, the actual extraterrestrial and circumsolar irradiances may depart from those predicted.

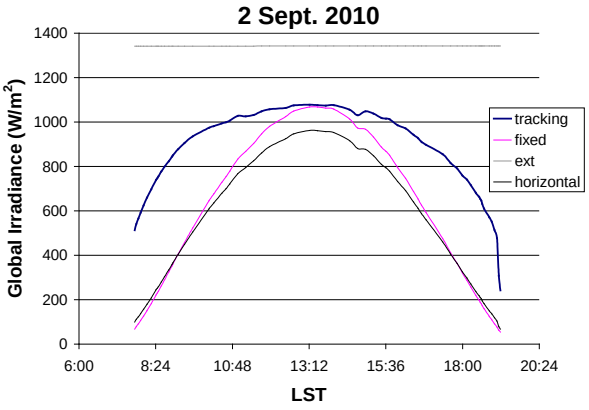

Fig. 9: Modeled irradiances incident on a tracking plane, fixed plane, horizontal plane and extraterrestrial based on AOD and water column using REST2.

5.2. PV Modeling

Using ECN IVFIT and IVGEN and measured PV electronic device characteristics, modeled irradiance was used to predict the power output of the two tested panels. At each time step, short circuit current was estimated to be proportional to the irradiance incident on each panel :

$$Isc = G\left(Isc_0 / G_0\right) \quad (3)$$

with G the incident global irradiance, and Isc_0 and G_0 reference current and irradiance from field characterization.

Temperature effects were not considered in the PV parameters. Temperature effects are a second-order correction to the fundamental irradiance response and temperature was not monitored. Also, PV parameters should be better characterized when using complex models. The Gummel-Poon model, for example, can model a wider variety of physical effects such as the Early effect [17,18].

The proportion of current to irradiance primarily shifts the i-v curve vertically, changing the intercept point of the two curves shown in Fig. 3, section 3. This process results in a non-linear load mismatch with irradiance and helps explain the steep slopes at low irradiance levels observed (Fig. 10).

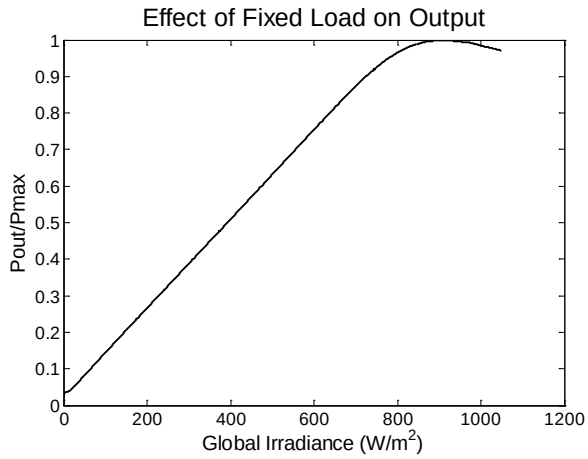

Fig. 10: Power out, Pout, varies in ratio with Pmax with irradiance. Pmax Watts would be obtained with a perfect MPPT tracking circuit.

In Figs. 11 and 12 below, while the analysis used explains observations qualitatively, two effects are worth mentioning. First, observed days with high, smooth PV panel output, suggested themselves for 'clear' classification, while in fact transient clouds and brief rain showers affected both spectrophotometer measurements and validity of the cloudless irradiance model used.

In the first case, cloud-screened Level 1.5 AERONET data are used here, as Level 2 quality assurance was not complete at the time of publication. Nevertheless, negative values of AOD at 1020nm appear at time steps near cloud passage. In the second case, the REST2 model is parameterized for alpha values below 2.5, while the fitting performed often resulted in values as large as 4 or 5.

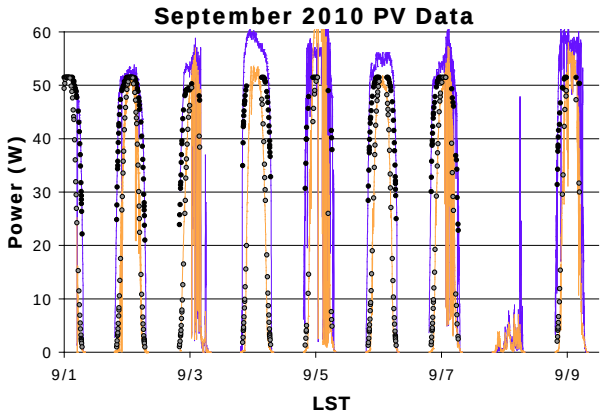

Fig. 11: Modeled performance plotted over measured performance time series.

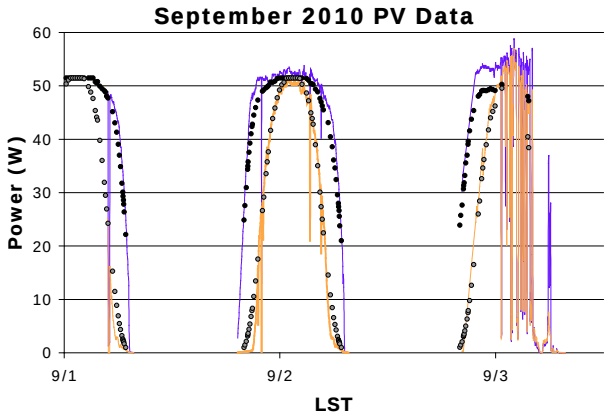

Fig. 12: Detail of model and measurement comparison, showing output behavior of PV panels driving fixed resistive loads.

Actual atmospheric conditions, such as deviation from predicted extraterrestrial irradiance or lensing effects due to slight cloud coverage near the solar disc may result in irradiances higher than those predicted by AOD and the cloudless sky REST2 model.

Shading from roofline and horizon was considered and eliminated as an explanation for power output behavior using another simple non-linear model [19].

6. CONCLUSION

Automating a solar tracker began as an educational project, and the ongoing analysis illustrates several areas to explore physical models that are replacing lumped parameter empirical fits which have limited applicability. The AERONET site provided atmospheric aerosol optical depth measurements that served as essential inputs to the physical understanding of the experiment.

By using REST2 and IVFIT to study how illumination influences electronic device characteristics, it was possible to determine that observed behavior of power output was due to load mismatch and not shading as initially supposed. Existing models were used to obtain more generally useful results.

Trackers are important technology supporting the development of solar energy, both for flat panel PV as studied here, as well as cutting edge concentrating solar technologies. It is essential to make students familiar with tracking practices, as a foundation for further research and development in this field.

7. ACKNOWLEDGMENTS

At Appalachian State University: Dana Greene, Mike Hughes, and Butch Miller are thanked for collaboration in instrumentation. Dr. Rahman Tashakorri and the NSF Academy of Sciences engaged and supported several students to do the work, and Nathan Kelischek to present at this conference. Jay Phillips acknowledges support of an Energy Center Research Grant to purchase microcontrollers. Thanks to Dr. Jim Sherman and AppalAir collaborators.

8. REFERENCES

(1) National Academy of Engineering, Grand Challenges for Engineering, http://www.engineeringchallenges.org
(2) US Energy Information Administration, http://www.eia.doe.gov/
(3) J. Cockman, A Dual Axis Solar Position Calculator and Tracker, AppState, (2005) MS Thesis
(4) S. Lamb, An Ephemeris Based Dual-Axis Solar Tracker Using the Basic Stamp Microcontroller, AppState, (2005), MS Report
(5) S. Lamb, A Fresnel Lens Based Concentrating PV Module, AppState, (2006), MS Reports
(6) http://www.arduino.cc/
(7) NOAA Solar Position Calculator, http://www.srrb.noaa.gov/highlights/sunrise/azel.html/
(8) Ruhi, Bharti, et. al., Nominal Operation Cell Temperature (NOCT): Effects of module size, power, load and solar spectrum, Photovoltaic Testing Laboratory, Arizona State University, (2005)
(9) G. Quéméré, R. Cervantes, J.M. Moreno, I. Luque-Heredia, Automation of the Calibration Process in the SUNDOG STCU, Conference Record of the 2006 IEEE 4th World Conference on Photovoltaic Energy Conversion (2006)
(10) AppalAir, http://www.appalair.appstate.edu/
(11) CIMEL Sunphotometers, http://www.cimel.fr
(12) AERONET (AErosol RObotic NETwork) program, http://aeronet.gsfc.nasa.gov/
(13) C. Gueymard, REST2: High-performance solar radiation model for cloudless-sky irradiance, illuminance, and photosynthetically active radiation – Validation with a benchmark dataset, Solar Energy 82 (2008) 272–285
(14) A. Burgers, J. Eikelboom, A. Schonecker, and W. Sinke, Improved treatment of the strongly varying slope in fitting solar cell I-V curves, Proc. 25th IEEE PVSC, (1996)
(15) A. R. Burgers, Fitting flash test curves with ECN's I-V Curve fitting Program IVFIT, Proc. 14th IEEE PVSC, (2004)
(16) Ozone Watch, http://ozonewatch.gsfc.nasa.gov/
(17) P. Horowitz and W. Hill, The Art of Electronics, Cambridge (1989)
(18) S. Sze, Semiconductor Devices, Wiley, (2001)
(19) N. Thakkar, D. Cormode, V. Lonij, S. Pulver and A. Cronin, A Simple Non-linear Model for the Effect of Partial Shade on PV Systems, Proc. 35th IEEE PVSC, (2010)